J. For. Res. (2023) 34:1747–1761
https://doi.org/10.1007/s11676-023-01620-7

ORIGINAL PAPER

Assessing fire severity in Turkey's forest ecosystems using spectral indices from satellite images

Coşkun Okan Güney[1] · **Ahmet Mert**[2] · **Serkan Gülsoy**[3]

Received: 27 December 2022 / Accepted: 27 March 2023 / Published online: 24 May 2023

Abstract Fire severity classifications determine fire damage and regeneration potential in post-fire areas for effective implementation of restoration applications. Since fire damage varies according to vegetation and fire characteristics, regional assessment of fire severity is crucial. The objectives of this study were: (1) to test the performance of different satellite imagery and spectral indices, and two field—measured severity indices, CBI (Composite Burn Index) and GeoCBI (Geometrically structured Composite Burn Index) to assess fire severity; (2) to calculate classification thresholds for spectral indices that performed best in the study areas; and (3) to generate fire severity maps that could be used to determine the ecological impact of forest fires. Five large fires in *Pinus brutia* (Turkish pine) and *Pinus nigra* subsp. *pallasiana* var. *pallasiana* (Anatolian black pine)—dominated forests during 2020 and 2021 were selected as study sites. The results show that GeoCBI provided more reliable estimates of field—measured fire severity than CBI. While Sentinel-2 and Landsat-8/OLI images performed similarly well, MODIS performed poorly. Fire severity classification thresholds were determined for Sentinel-2 based RdNBR, dNBR, dSAVI, dNDVI, and dNDMI and Landsat-8/OLI based dNBR, dNDVI, and dSAVI. Among several spectral indices, the highest accuracy for fire severity classification was found for Sentinel-2 based RdNBR (72.1%) and Landsat-8/OLI based dNBR (69.2%). The results can be used to assess and map fire severity in forest ecosystems similar to those in this study.

Keywords Remote sensing · Forest fire · Fire severity · Spectral indices · Composite burn index

Project Funding: This project was funded by the Turkish General Directorate of Forestry (project number: 19.9402/2020-2023).

The online version available at http://www.springerlink.com.

Corresponding editor: Yu Lei.

Supplementary Information The online version contains supplementary material available at https://doi.org/10.1007/s11676-023-01620-7.

✉ Coşkun Okan Güney
coskunokanguney@ogm.gov.tr

1 Department of Forest Fires, Aegean Forestry Research Institute, 35430 Izmir, Turkey

2 Department of Wildlife Ecology and Management, Faculty of Forestry, Isparta University of Applied Science, 32260 Isparta, Turkey

3 Department of Soil Science and Ecology, Faculty of Forestry, Isparta University of Applied Science, 32260 Isparta, Turkey

Introduction

In many areas of the world, large forest fires have become more frequent in recent years. It is expected that there will be an increase in the number of forest fires and amount of burned areas due to climate change and increases in world population (Amatulli et al. 2013). However, fires are a natural process that affect ecosystems (Whitman et al. 2015) and influence biophysical processes at different temporal and spatial scales, from micro-scale impacts (e.g., on a single plant) to broad landscape patterns and processes (Cochrane and Ryan 2009). Forest areas that do not burn or are exposed to low-intensity fires and do not lose vitality contribute to biodiversity by creating heterogeneous spatial structures (Turner and Romme 1994). To preserve this biodiversity, post fire-management should follow a sustainable ecological approach (Baysal et al. 2016). A good way to accurately characterize burned areas is to determine fire severity, considered as the degree of ecological change in both vegetation and soil caused by fire (Kasischke and Bruhwiler 2002). Fire severity is generally accepted as a measure of fuel consumption and mortality. "Fire severity" and "burn severity" are used to determine the extent of environmental change caused by fire (Keeley 2009). The two terms have different ecological and temporal meanings. Fire severity describes short-term effects, while burn severity describes the long-term effects on ecosystems and vegetation (French et al. 2008). While fire severity is assessed immediately or within the first 30–45 days after a fire event (Key and Benson 2006), burn severity may be estimated at different times and seasons (Key 2006).

Fires often occur in large areas which can result in damage assessments taking considerable effort, money, and time. Therefore, remote sensing methods are frequently used after large fires to determine the extent of damage to ecosystems (Key and Benson 2006). Satellite data such as Sentinel-2, Landsat-8/OLI, and MODIS provide the most widely used free imagery datasets for monitoring (Song et al. 2021). Since remote sensing data provide a quantitative assessment of vegetation and soil-related information, these data are also used for fire severity assessment (Luo and Wu 2022).

Depending on the resolution of satellite sensors, several satellite-based spectral indices can be correlated with data from field measurements. The most commonly used indices to detect fire effects through remote sensing are the Normalized Difference Vegetation Index (NDVI) (Mallinis et al. 2018; Ba et al. 2020), the Normalized Burn Ratio (NBR) (Lutes et al. 2006; Miller and Thode 2007; Fernández-García et al. 2018; Ba et al. 2020), the Enhanced Vegetation Index (EVI) (Wu et al. 2015; Ba et al. 2020), the Soil Adjusted Vegetation Index (SAVI) (Wu et al. 2015), the Global Environment Monitoring Index (GEMI) (Ba et al. 2020), the Normalized Difference Water Index (NDWI) (Beltrán-Marcos et al. 2021), the Normalized Difference Moisture Index (NDMI) (Choubin et al. 2017), the Burned Area Index (BAI) (Chuvieco et al. 2002; Ba et al. 2020), the Burned Area Index Modified–LSWIR (BAIML) (Fornacca et al. 2018), the Burned Area Index Modified-SSWIR (BAIMS) (Fornacca et al. 2018), the Mid Infrared Burn Index (MIRBI) (McCarley et al. 2018), Char Soil Index (CSI) (Pletsch et al. 2019; Ba et al. 2020), Relative differenced Normalized Burn Ratio (RdNBR), and Relativized Burn Ratio (RBR) (Parks et al. 2014). Spectral reflectance values from remote sensing satellite images depend on fire characteristics and vegetation type (French et al. 2008). Severity varies with fire intensity, residence time, tree sizes and species-related physiological characteristics (Michaletz and Johnson 2007; Valor et al. 2017). This results in different spectral responses and therefore different fire severity values that need to be calibrated (Miller and Quayle 2015). To produce fire severity maps from satellite images alone, without the knowledge of site or vegetation conditions, is difficult. Therefore, calibrations using field measurements are necessary. The most widely used method is the Composite Burn Index (CBI) developed by Key and Benson (2006). The CBI divides the forest into five vertical strata and rates them with numerical scores from 0 (unburned) to 3 (completely burned) based on the visual assessment of the amount of fuel consumed, degree of soil scorched, blackening or scorching of trees, and plant regeneration (Key and Benson 2006). In previous studies, the CBI correlated well with spectral reflectance values of remote sensing data (Soverel et al. 2010; Cansler and McKenzie 2012). However, De Santis and Chuvieco (2009) found that the CBI was inconsistent and worked well in some ecosystems but not in others. Therefore, they proposed a modified version, the Geometrically structured Composite Burn Index (GeoCBI). The difference between the CBI and the GeoCBI is that the latter also estimates the fraction of vegetation cover (FCOV). Hence, it is more consistently related to spectral reflectance values than the CBI (De Santis and Chuvieco 2009).

Researchers from different countries have identified spectral thresholds for discriminating fire severity classes in different vegetation types such as steppe (White et al. 1996), tundra (Zhu et al. 2006; Allen and Sorbel 2008), savannah (Alleaume et al. 2005; Borini Alves et al. 2018), meadows (White et al. 1996; Rogan and Franklin 2001), shrubs (White et al. 1996; Epting et al. 2005), temperate forests (French et al. 2008), coniferous forests (Miller and Thode 2007; Mallinis et al. 2018), and deciduous forests (Zhu et al. 2006).

However, only a limited number of studies have investigated the relationship between fire severity data from remote sensing and field measurements of forested areas with dense vegetation cover in the Mediterranean basin, although it is a region heavily affected by forest fire (Lasaponara et al. 2006; Mallinis et al. 2018; Saulino et al. 2020). Further studies are needed that assess fire severity based on regional field measurements correlated with satellite imagery in Mediterranean forest ecosystems (Epting et al. 2005; Hudak et al. 2007; Mallinis et al. 2018).

The purpose of this study was to accurately map fire severity in forest ecosystems of Turkey using local thresholds for the first time. The specific objectives were: (1) to evaluate the performance of different satellite imagery, spectral indices, and field measurements; and (2) to determine classification thresholds of best-performing spectral indices in order to generate fire severity maps to determine the ecological effects of fires in different fire-prone forest ecosystems.

Materials and methods

Study area

This study focused on five forest fires that occurred during 2020 and 2021 (Table 1). Three (Adana-Kozan, Denizli-Çardak, and Antalya-Manavgat) were within the Mediterranean climate region in southern Turkey (Fig. 1), an area at highest risk of forest fires. The other two fires were in Ankara-Nallıhan (western Inner Anatolia) and Kastamonu-Taşköprü (western Black Sea region), both within the western Black Sea climate zone with high fire risk. All fires occurred during the fire season when fire weather conditions prevailed. Fires were selected that had occurred in forests dominated by Turkish pine (*Pinus brutia* Ten.) and/or Anatolian black pine (*Pinus nigra* Arn. subsp. *pallasiana* (Lamb.) Holmboe var. *pallasiana*), as they are the two main forest types in Turkey most affected by fires. These forests are occasionally mixed with broad-leaved species and maquis shrubland species. The sites were heterogeneous in terms of topography and vegetation.

Imagery and preprocessing

Sentinel-2, Landsat-8/OLI, and MODIS satellite images are freely available and used in this study. Cloudless pre- and post-fire images closest to the fire dates were selected. Imageries were downloaded from USG Earth Explorer server. The Sentinel satellite consists of 13 bands with a revisiting time of 10 days. Landsat-8/OLI is 11 bands with a revisiting time of 16 days while MODIS is 7 bands with a revisiting time of 8 days (Table 2).

Preprocessing of satellite data included geometric (Itten and Meyer 1993), radiometric (Teillet 1986), and atmospheric (Kaufman and Sendra 1988) corrections. Data were first defined in the same coordinate system using the Universal Transverse Mercator projection and WGS84 datum. Geometric corrections included the elimination of distortions between satellite data using ground control points. Among the geometrically corrected data, the root-mean-square error (RMSE) should be lower than 0.5 (Lunetta and Elvidge 1999). Landsat-8/OLI Collection 2 Level 1 satellite data were downloaded using the Digital Elevation model

Table 1 Vegetation and climate characteristics of the study areas

1. Adana-Kozan Fire	Fire date: 23.08.2020
Burned area	4201 ha
Main plant species	*Pinus brutia, Ceratonia siliqua* L., *Olea europaea* L., *Nerium oleander* L., *Myrtus communis* L., *Cistus creticus* L
Climate characteristics	Mean annual temperature: 19.5 °C
	Total annual precipitation: 680.8 mm
2. Ankara-Nallıhan Fire	Fire date: 01.09.2020
Burned area	1229 ha
Main plant species	*Pinus nigra* subsp. *pallasiana* var. *pallasiana*, *Quercus pubescens* Willd., *Platanus orientalis* L., *Erica arborea* L
Climate characteristics	Mean annual temperature: 12.6 °C
	Total annual precipitation: 413.6 mm
3. Kastamonu-Taşköprü Fire	Fire date: 02.09.2020
Burned area	1681 ha
Main plant species	*Pinus nigra* subsp. *pallasiana* var. *pallasiana*, *Pinus sylvestris* L., *Populus tremula* L., *Quercus petraea* (Matt.) Liebl.,
Climate characteristics	Mean annual temperature: 10.1 °C
	Total annual precipitation: 525.3 mm
4. Denizli-Çardak Fire	Fire date: 03.09.2020
Burned area	401 ha
Main plant species	*Pinus brutia*, *Pinus nigra* subsp. *pallasiana* var. *pallasiana*, *Juniperus excelsa* M. Bieb., *Quercus coccifera* L., *Arbutus andrachne* L., *Pistacia terebinthus* L
Climate characteristics	Mean annual temperature: 16.9 °C
	Total annual precipitation: 573.8 mm
5. Antalya-Manavgat Fire	Fire date: 28.07.2021
Burned area	60,362 ha
Main plant species	*Pinus brutia*, *Pinus nigra* subsp. *pallasiana* var. *pallasiana*, *Pinus pinea* L, *Juniperus excelsa, Cupressus sempervirens* L., *Ceratonia siliqua* L., *Quercus coccifera*, *Laurus nobilis* L., *Myrtus communis* L
Climate characteristics	Mean annual temperature: 19.0 °C
	Total annual precipitation: 1059.4 mm

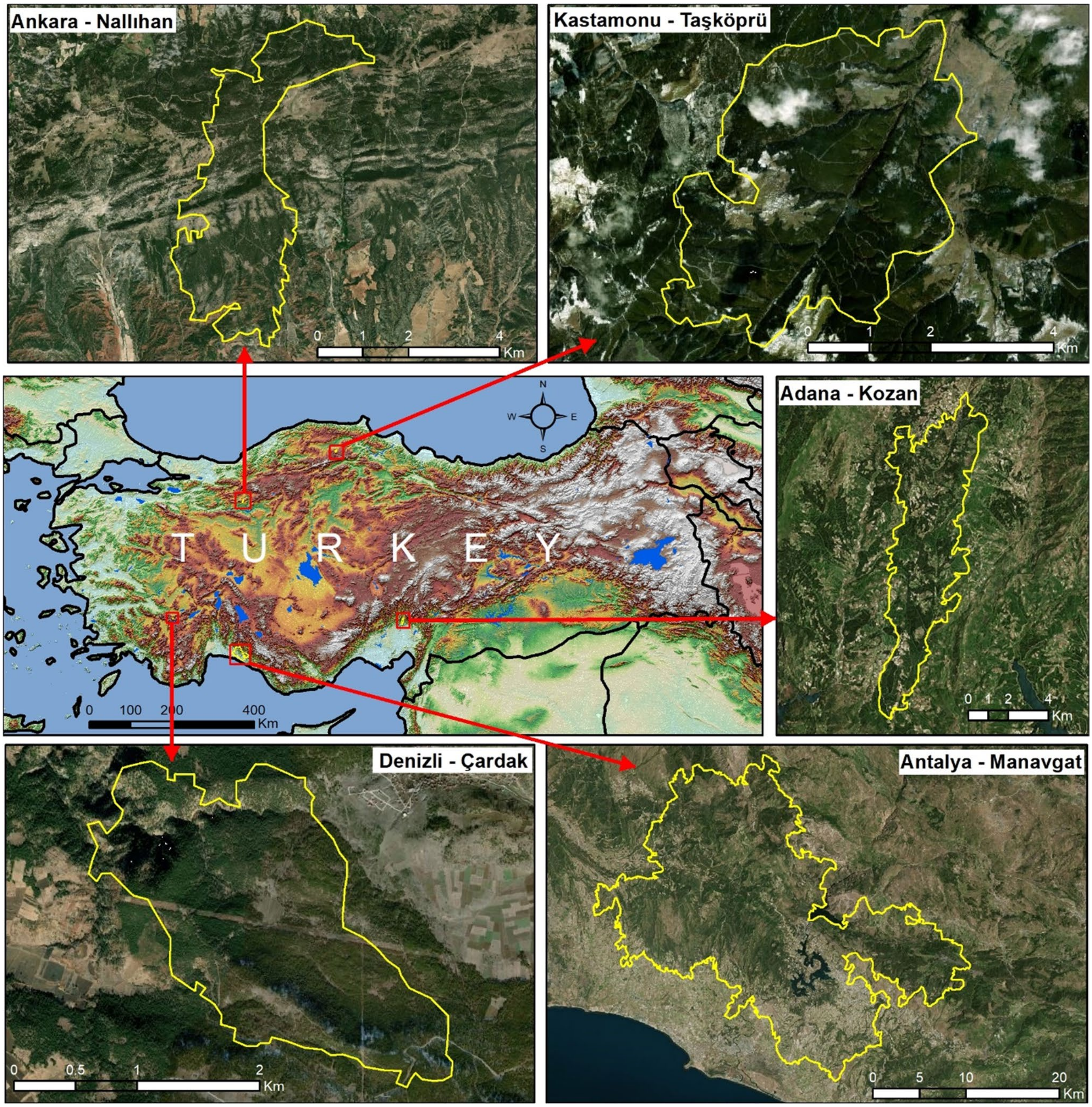

Fig. 1 Location of the burned areas

with radiometric and geometric corrections already applied. Geometric, radiometric, and atmospheric corrections of Sentinel-2 satellite data were made using the Sentinel-2 toolbox (Gascon and Ramoino 2017).

After the data were geometrically corrected, a RMSE of 0.44 was calculated. Radiometric corrections included the elimination of atmospheric effects that might cause data errors and the radiometric calibration of pixels that do not represent reflectance values. Atmospheric corrections used the extrapolated Rayleigh-corrected reflectance at NIR and SWIR bands to derive their ratios and visible aerosol single scattering contributions (aerosol epsilon). FLAASH (Fast Line-of-sight Atmospheric Analysis of Hypercubes) and flat field were used for atmospheric corrections to remove effects such as aerosols and water vapor from satellite data (Matthew et al. 2002; Ye et al. 2016; Ilori et al. 2019). After these corrections were completed, spectral indices from the literature (Table 3) were

Table 2 Spectral characteristics used for estimating fire severity (Fernández-Manso et al. 2016; Choubin et al. 2017; Korhonen et al. 2017)

Sentinel-2			Landsat-8/OLI			MODIS		
Spectral bands	Wavelength range (nm)	Resolution (m)	Spectral bands	Wavelength range (nm)	Resolution (m)	Spectral bands	Wavelength range (nm)	Resolution (m)
B1-Coastal aerosol	433–453	60	B1-Coastal aerosol	433–453	30	B1-Red	620–670	250
B2-Blue	458–523	10	B2-Blue	450–515	30	B2-NIR	841–876	250
B3-Green	543–578	10	B3-Green	525–600	30	B3-Blue	459–479	500
B4-Red	650–680	10	B4-Red	630–680	30	B4-Green	545–565	500
B5-Red Edge1	698–713	20	B5-NIR	845–885	30	B5-SWIR1	1230–1250	500
B6-Red Edge2	733–748	20	B6-SSWIR-1	1560–1660	30	B6-MIR, SWIR2	1628–1652	500
B7-Red Edge3	773–793	20	B7-LSWIR-2	2100–2300	30	B7-MIR, SWIR3	2105–2155	500
B8-NIR	785–900	10	B8-Pan	500–680	15			
B8a-NIRn	855–875	20	B9-Cirrus	1360–1390	30			
B9-Water vapour	935–955	60	B10-TIR1	10 300–10,100	100			
B10-SWIR / Cirrus	1360–1390	60	B11-TIR2	11,500–12,500	100			
B11-SSWIR	1565–1655	20						
B12-LSWIR	2100–2280	20						

Table 3 Spectral indices used for estimating fire severity

Spectral index	Equation	References
NDVI	$NDVI = \frac{NIR-R}{NIR+R}$	Tucker (1979)
NBR	$NBR = \frac{NIR-LSWIR}{NIR+LSWIR}$	Lutes et al. (2006)
EVI	$EVI = 2,5\frac{NIR-R}{NIR-6R-7,5B+1}$	Huete et al. (2002)
SAVI	$SAVI = (1+L)\frac{NIR-R}{NIR+R+L}L = 0,5$	Huete (1988)
BAI	$BAI = \frac{1}{(0,1+R)^2+(0,06+NIR)^2}$	Chuvieco et al. (2002)
MIRBI	$MIRBI = 10LSWIR - 9,8SSWIR + 2$	Trigg and Flasse (2001)
CSI	$CSI = \frac{NIR}{SWIR2}$	Smith et al. (2007)
GEMI	$GEMI = y(1-0,25y) - \frac{R-0,125}{1-R}$ $y = \frac{2\left(NIR^2-R^2\right)+1,5NIR+0,5R}{NIR+R+0,5}$	Pinty and Verstraete (1992)
NDWI	$NDWI = \frac{NIR-SWIR1}{NIR+SWIR1}$	Gao (1996)
NDMI	$NDMI = \frac{NIR-SWIR}{NIR+SWIR}$	Wilson and Sader (2002)
BAIML	$BAIM = \frac{1}{(NIR-0,05xNIR)^2+(LSWIR-0,2xLSWIR)^2}$	Fornacca et al. (2018)
BAIMs	$BAIMS = \frac{1}{(NIR-0,05xNIR)^2+(sSWIR-0,2xsSWIR)^2}$	Fornacca et al. (2018)
RdNBR	$RdNBR = \frac{dNBR}{\sqrt{\left\|\left(\frac{NBR_{prefire}}{1000}\right)\right\|}}$	Miller and Thode (2007)
RBR	$RBR = \frac{dNBR}{(NBR_{prefire}+1,001)}$	Parks et al. (2014)

MIR mid infrared, *R* RED, *NIR* near infrared, *SSWIR* shorter short-wave infrared, *LSWIR* longer short-wave infrared calculated using pre- and post-fire satellite images and the Raster Calculator tab within the ArcMap software. Fire severity maps were generated from the differences between the two images (Mallinis et al. 2018; Saulino et al. 2020) (Table S1).

Field sampling

Fire severity measurements were conducted within 5–45 days following the fire. Sampling plots were randomly selected within the burned area using the stratified random sampling approach. It was ensured that the number of plots was proportional to the area each fire class covered. A total of 478 sampling plots were determined. Depending on the burn size, the number of plots for the Adana-Kozan fire was 70, 60 for Ankara-Nallıhan, 105 for Kastamonu-Taşköprü, 15 for Denizli-Çardak, and 228 for the Antalya-Manavgat fire. At each 30 × 30 m sampling plot, fire severity conditions were visually assessed according to the CBI field protocol proposed by Key and Benson (2006) for all five strata by assigning each a value from 0 (unburned) to 3 (severely burned) (Table 4). At the center of each plot, digital images covering different angles were acquired and GPS coordinates were recorded. The GeoCBI for each plot was assessed following the protocol described by De Santis and Chuvieco (2009).

Table 4 Measured CBI and GeoCBI values of different fire severity classes on some of the sampling plots

Adana-Kozan	Ankara-Nallıhan	Kastamonu-Taşköprü	Denizli-Çardak	Antalya-Manavgat
	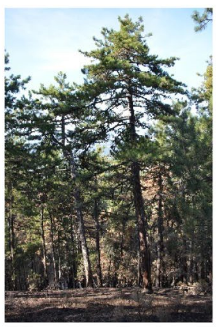			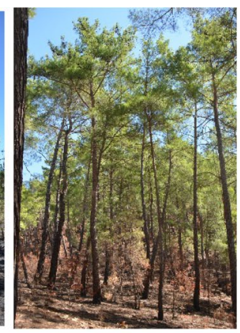
CBI: 1.33 GeoCBI: 1.10	CBI: 0.82 GeoCBI: .0.72	CBI: 1.07 GeoCBI: 0.96	CBI: 1.19 GeoCBI: 1.09	CBI: 0.79 GeoCBI: 0.38
	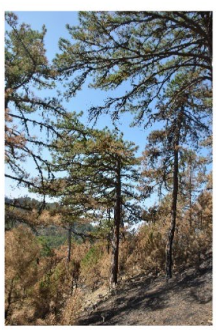	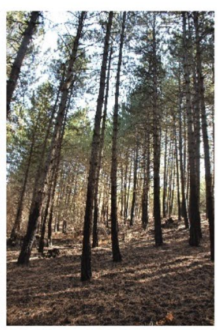		
CBI: 1.96 GeoCBI: 1.88	CBI: 1.91 GeoCBI: 1.88	CBI: 1.86 GeoCBI: 1.32	CBI: 1.84 GeoCBI: 1.17	CBI: 1.57 GeoCBI: 1.41
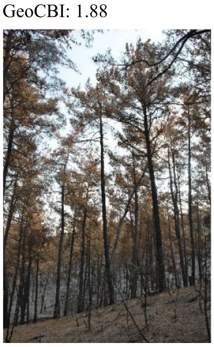				
CBI: 2.70 GeoCBI: 2.63	CBI: 2.38 GeoCBI: 2.36	CBI: 2.70 GeoCBI: 2.48	CBI: 3.00 GeoCBI: 3.00	CBI: 2.84 GeoCBI: 2.80

Relationship between remote sensing and field-measured fire severity

To determine the relationships between field-measured fire severity and the spectral indices from satellite imageries, Kendall's correlation analysis was performed. Based on these results, subsequent analyses were only performed for GeoCBI and spectral indices from Sentinel-2 and Landsat-8/OLI satellite imageries. Linear regression analysis was used to determine the relationship between GeoCBI and the spectral indices with the highest Kendall's correlation coefficient (Escuin et al. 2008; Mallinis et al. 2018; García-Llamas et al. 2019).

Defining threshold values for spectral indices

Threshold values were determined for best performing spectral indices. For this, optimal binning analysis was carried out using SPSS for spectral indices with the highest R^2 derived from Sentinel-2 and Landsat-8/OLI satellite images. In order to classify the values of the spectral indices, the classification proposed by Miller et al. (2009) was used: unburned (0–0.1), low (0.1–1.25), moderate (1.26–2.25), and high (2.26–3.0). This approach allowed for the identification of reflectance threshold values of the most suitable spectral indices based on the locally measured GeoCBI classification. Kappa statistics were then used to assess agreement between GeoCBI classes and optimized classified threshold values. In addition, for each of these spectral indices, a comparison was made between the predicted classes and those obtained via field measurements, and prediction accuracy percentages were calculated (Tables S2 and S3).

Results and discussion

According to our results, spectral indices from both Sentinel-2 and Landsat-8/OLI satellite imageries correlated best with the GeoCBI measurements. After De Santis and Chuvieco (2009) suggested the use of GeoCBI, noting that CBI does not work well in some regions and/or vegetation types, some studies either used GeoCBI instead of CBI or both, to test which one correlates better with spectral reflectance values. Consistent with our results, Mallinis et al. (2018) found in their study from Greece, that GeoCBI was better correlated with spectral indices from both Landsat-8/OLI and Sentinel-2 satellite imagery than CBI. In a study from Australia (Parker et al. 2015), the dNBR spectral index from Landsat satellite images showed a strong correlation with GeoCBI. However, Cansler and McKenzie (2012) in the USA showed that the use of CBI led to better results than GeoCBI. Saulino et al. (2020), on the other hand, reported that spectral indices from Landsat-8/OLI correlated better with CBI while spectral indices from Sentinel-2 were better correlated with GeoCBI.

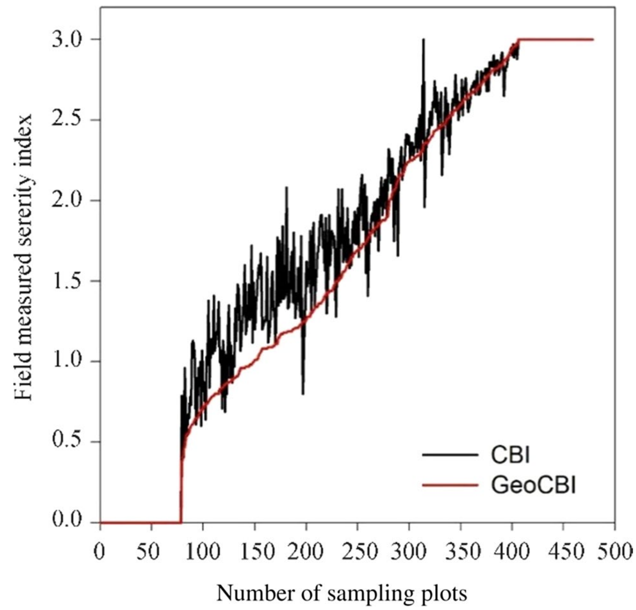

Fig. 2 Comparison of CBI and GeoCBI values obtained for the respective sampling plots

Of the 478 fire severity sampling plots from five different fire areas, 78 were unburned, 62 were lightly burnt, 152 were moderately burnt, and 186 showed high fire severity. In general, GeoCBI scores were lower than CBI scores for these sampling sites (Fig. 2). In cases where the sampling plots were unburned or all strata showed similar fire severity, CBI and GeoCBI were the same or similar to each other. However, in cases where the ground cover showed high fire severity but the upper crown layer remained unburned, GeoCBI resulted in lower values than CBI (Table 4). This is because GeoCBI is calculated by weighing each layer (stratum) according to its estimated coverage within the plot. Further, if the upper canopy is dense, it causes most of the satellite observed reflectance (De Santis and Chuvieco 2009). Considering only the upper or lower stratum during fire severity classification can lead to incorrect results. It may therefore be concluded that, in cases where the upper canopy is dense and the level of damage is low, GeoCBI provides a better characterization of fire severity.

Of the three different satellite data used in this study, Sentinel-2 and Landsat-8/OLI were more closely correlated with field measurement data than MODIS (Table 5). Further, although Landsat-8/OLI has a lower resolution (30 m) than Sentinel-2 (10 m), it provided better results for some of the indices due to its higher resolution, but since the differences between results are usually minor, both Sentinel-2 and Landsat-8/OLI can be used (Mallinis et al. 2018; Saulino et al. 2020). Correlation coefficients between MODIS and field

Table 5 Kendall's correlation coefficients between spectral indices and field measurements (CBI and GeoCBI)

Spectral indices	CBI			GeoCBI		
	Sentinel-2	Landsat-8/OLI	MODIS	Sentinel-2	Landsat-8/OLI	MODIS
dNDVI	0.68	0.68	0.37	**0.68**	**0.69**	0.38
dNBR	0.74	0.69	0.39	**0.75**	**0.70**	0.39
dEVI	0.56	0.62	0.16	0.56	0.62	0.15
dSAVI	0.69	0.68	0.10	**0.69**	**0.69**	0.11
dBAI	0.14	0.62	0.11	0.13	0.07	0.12
dMIRBI	0.53	0.48	0.36	0.54	0.49	0.37
dCSI	0.59	0.49	0.37	0.59	0.48	0.38
dGEMI	0.53	0.41	0.32	0.52	0.40	0.33
dNDWI	0.68	0.68	0.34	**0.68**	**0.69**	0.35
dNDMI	0.69	0.67	0.38	**0.69**	0.67	0.38
dBAIML	0.58	0.47	0.21	0.58	0.48	0.21
dBAIMS	0.29	0.35	0.03	0.30	0.34	0.05
RdNBR	0.74	0.70	0.41	**0.74**	**0.70**	0.42
dRBR	0.20	0.21	0.13	0.19	0.20	0.15

All correlations are statistically significant at 0.05 level. Highest correlations are in bold

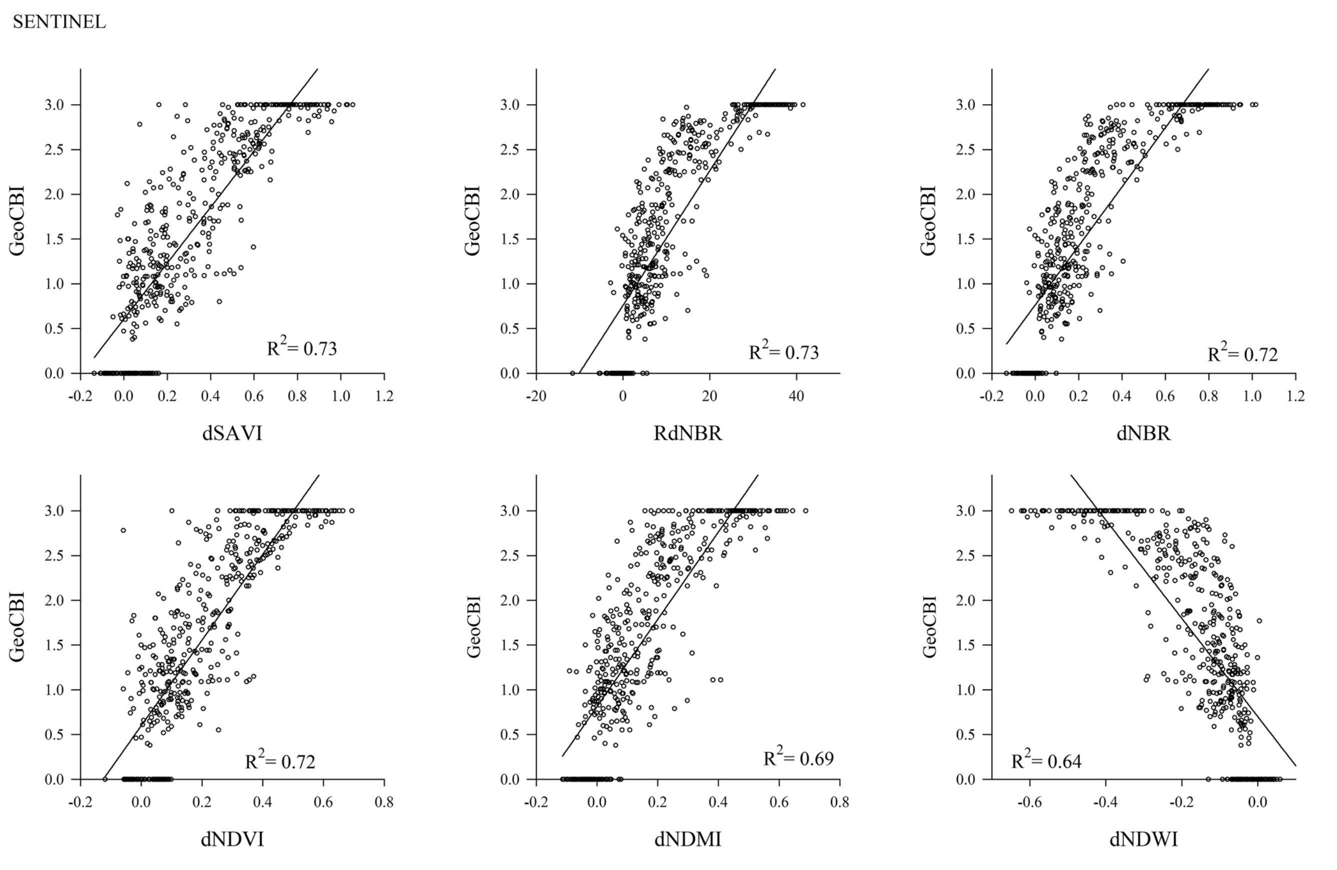

Fig. 3 Linear regression between spectral indices (dSAVI, RdNBR, dNBR, dNDVI, dNDMI and dNDWI) from Sentinel-2 satellite images and GeoCBI

measurements were significantly lower for most spectral indices (Table 5), possibly because of the low resolution of MODIS satellite images (250 m).

Linear regression was performed to determine the relationship between the spectral indices that resulted in the highest correlation coefficients (Table 5) and GeoCBI

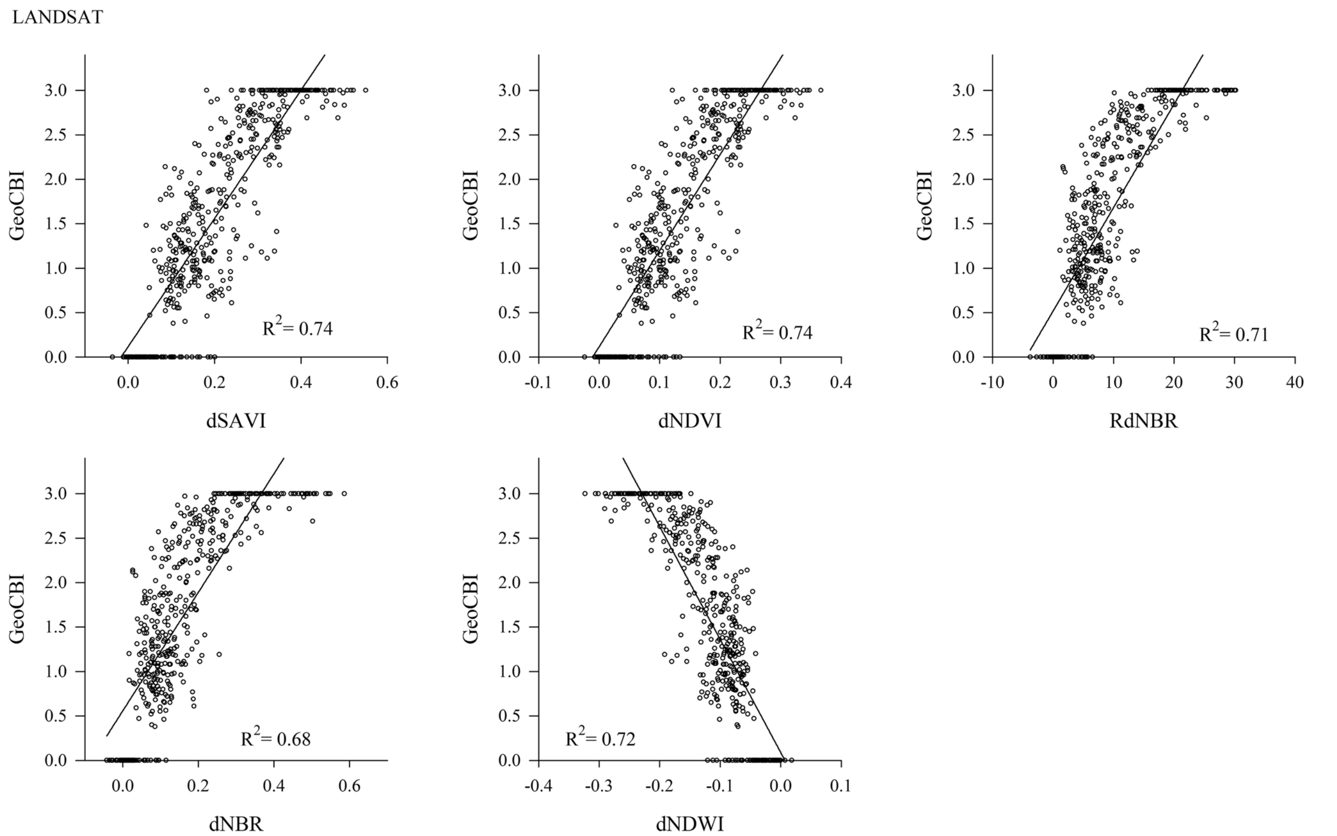

Fig. 4 Linear regression between spectral indices (dSAVI, dNDVI, RdNBR dNBR, and dNDWI) from Landsat-8/OLI satellite images and GeoCBI

Table 6 Threshold values of the spectral indices from Sentinel-2 satellite images

SENTINEL-2					
GeoCBI Classes	dSAVI	RdNBR	dNBR	dNDVI	dNDMI
Unburned	< −0.030	< 0.541	< 0.012	< 0.099	< −0.014
Low	−0.030 to 0.161	0.541 to 7 641	0.013 to 0.099	0.100 to 0.180	−0.015 to 0.110
Moderate	0.162 to 0.371	7 642 to 10 292	0.100 to 0.219	0.181 to 0.292	0.111 to 0.239
High	> 0.371	> 10 292	> 0.219	> 0.292	> 0.239

Table 7 Threshold values of spectral indices from Landsat-8/OLI satellite images

LANDSAT-8			
GeoCBI Classes	dSAVI	dNDVI	dNBR
Unburned	< 0.072	< 0.048	< 0.034
Low	0.072–0.150	0.049–0.103	0.035–0.129
Moderate	0.151–0.251	0.104–0.167	0.130–0.172
High	> 0.251	> 0.167	> 0.172

values (Figs. 3 and 4). The ones with the highest coefficients of determination (R^2) were dSAVI ($R^2 = 0.73$), and RdNBR ($R^2 = 0.73$) for the Sentinel-2 data as well as dNDVI ($R^2 = 0.74$) and dSAVI ($R^2 = 0.74$) for the Landsat-8/OLI data.

Based on the GeoCBI classification, fire severity thresholds of the best-performing spectral indices were calculated using optimal binning analysis. Optimal classification was performed for five spectral indices (except dNDWI) derived from Sentinel-2 (Table 6) and for three spectral indices (dSAVI, dNDVI, and dNBR) from Landsat-8/OLI (Table 7).

According to the literature, most fire severity studies determine thresholds of Landsat dNBR. For example, regional dNBR classification thresholds were determined for Alaska (Epting et al. 2005), Montana, USA (Key and Benson 2006), California, USA (Miller and Thode 2007), Indonesia (Hoscilo et al. 2013), Australia (Parker et al.

2015), and Greece (Mallinis et al. 2018). The Landsat dNBR threshold values from our study are closest to those of Miller and Thode (2007) for California. Our results differ from those of Mallinis et al. (2018) for Greece, although their study was conducted in a *Pinus brutia* stand on Thasos Island which is close to Turkey with similar vegetation. Compared to other studies, our threshold classification values were overall lower. Regional differences can occur based on fire intensity, vegetation cover and species-specific reaction to the fire, leading to different reflectance values corresponding to the fire severity classes (Miller and Quayle 2015). Thresholds of spectral indices can perform well in terms of fire severity classification for a specific place and time but may not perform well elsewhere (Huang et al. 2016).

Based on Kappa statistics, the level of agreement between spectral indices and field GeoCBI was highest for Sentinel-2—based RdNBR (Kappa values for RdNBR: 0.653, dNBR: 0.622, dSAVI: 0.512, dNDMI: 0.506, and dNDVI: 0.001) and Landsat-8/OLI—based dNBR (Kappa values for dNBR: 0.603, dSAVI: 0.588, and dNDVI: 0.588).

Accuracy percentages were calculated between observed and predicted GeoCBI. For all fire severity classes, highest accuracy was for Sentinel-2—based RdNBR (72.1%) and Landsat-8/OLI—based dNBR (69.2%). RdNBR and dNBR showed highest accuracies for unburned, low, and high severity classes but lower accuracies for the moderate class (Tables S3 and S4). Some studies found that dNBR was less sensitive to consumption in the lower strata while the upper canopy was still green (Hoy et al. 2008; De Santis and Chuvieco 2009) but our results show that RdNBR and dNBR are also successful in the low severity class.

According to the results of this study, spectral indices showing the highest accuracy and agreement with field measured GeoCBI were Sentinel-2—based RdNBR and Landsat-8/OLI—based dNBR. In most of studies that tested the performance of spectral indices to estimate fire severity, NBR—based dNBR and RdNBR proved to be the best in detecting fire-caused changes (Epting et al. 2005; Escuin et al. 2008; Veraverbeke et al. 2011; Cansler and McKenzie 2012; Fernández-García et al. 2018; Ariza et al. 2019; García-Llamas et al. 2019). Other studies showed that RBR provides a more accurate estimation of fire severity than dNBR and RdNBR and thus the use of the spectral index RBR is suggested (Parks et al. 2014; Ariza et al. 2019). However, in our study, RBR performed poorly. The performance of NDVI, which was less than dNBR and RdNBR in our study, varied from superior (Chen et al. 2011) to good (García-Llamas et al. 2019) to poor (Fernández-García et al. 2018) in other studies. Hudak et al. (2007) found that the performance of dNDVI and dNBR were comparable and that both could be used for fire severity classification. In another study by Arnett et al. (2015) for a low-intensity prescribed fire in Canada, dSAVI was the best performing index among others calculated from both Landsat and Rapideye satellite images. They stated that dSAVI better represented areas of low-intensity fires and low fire severity. However, in this study, although dSAVI was among the indices showing the highest correlation with ground measurements for both Sentinel-2 and Landsat-8/OLI, overall agreement of dSAVI and field GeoCBI was inferior and its performance to accurately estimate fire severity classes was poor. dMIRBI is recommended for use in areas with low fire severity as it shows higher spectral separability, especially when a dense canopy is present (McCarley et al. 2018). Based on our results, we were not able to support this conclusion.

NDVI and SAVI are indices using NIR and RED bands, while NBR and NDMI use NIR and SWIR bands. With the reflectance values of the Landsat-8/OLI satellite images, it can be seen that spectral bands 4 (RED), 5 (NIR), 6 (SSWIR), and 7 (LSWIR) show high separability between fire severity classes (Fig. 5). With regards to the reflectance values of Sentinel-2, the bands that reached high separability were bands 4 (RED), 5 (RED Edge1), 6 (RED Edge2), 7 (RED Edge3), 8 (NIR), 8a (NIRn), 11 (SSWIR), and 12 (LSWIR) (Fig. 6). This agrees with results from other studies (Lewis et al. 2007; Papageorgiou et al. 2012; Pleniou and Koutsias 2013; Liu et al. 2016; Ariza et al. 2019; Chuvieco et al. 2019; Luo and Wu 2022) and our study as indices using these bands provided the best results. Overall, in our study, NBR-based RdNBR and dNBR indices were more successful in classifying fire severity than the other indices. This is because the NIR band is sensitive to chlorophyll levels, while SWIR is sensitive to plant and soil water contents

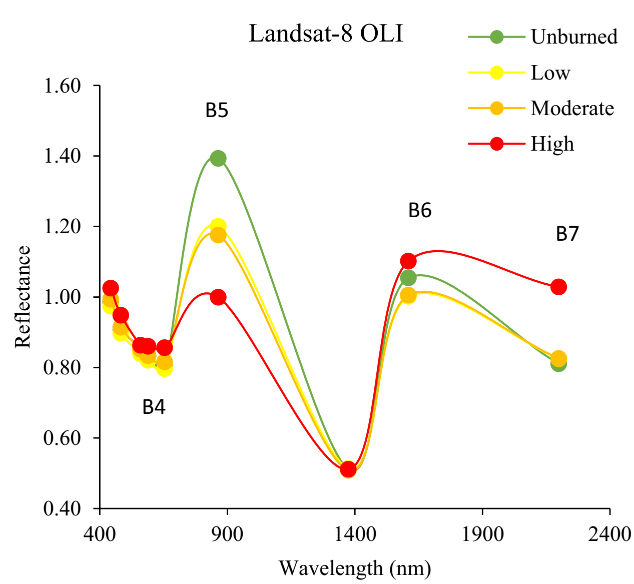

Fig. 5 Reflectance values of different fire severity classes according to Landsat-8/OLI satellite images (B indicates spectral bands)

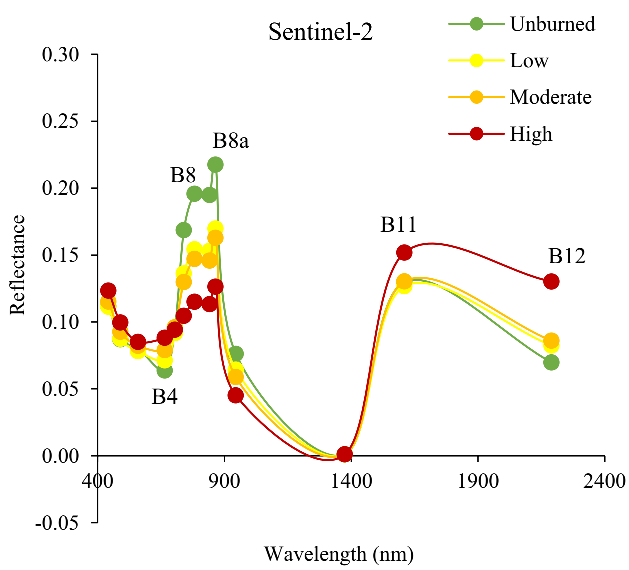

Fig. 6 Reflectance values of different fire severity classes according to Sentinel-2 satellite images (B indicates spectral bands)

as well as to the ash content after a fire (Miller and Thode 2007). However, although dNDVI and dSAVI were highly correlated with field measurements, they did not perform as well as RdNBR and dNBR in terms of fire severity classification. This is because RED bands, although sensitive to fire-related decreases in chlorophyll content, show only limited sensitivity to post-fire attributes such as black carbon or ash (García-Llamas et al. 2019). Further, the better performance of Sentinel-2 based RdNBR over dNBR may be explained by the differences in pre-fire chlorophyll levels and density of vegetation cover. Therefore, RdNBR allows for a more accurate estimate of fire severity in heterogeneous terrains (Miller and Thode 2007).

Fire severity maps were generated using the threshold values calculated for the Sentinel-2—based RdNBR (Fig. 7) and Landsat—based dNBR indices (Fig. 8). For all fires, the majority of the burned areas were classified as high fire severity (Tables S4 and S5). This was expected for fires that occurred during the fire season and during periods of extreme fire weather conditions.

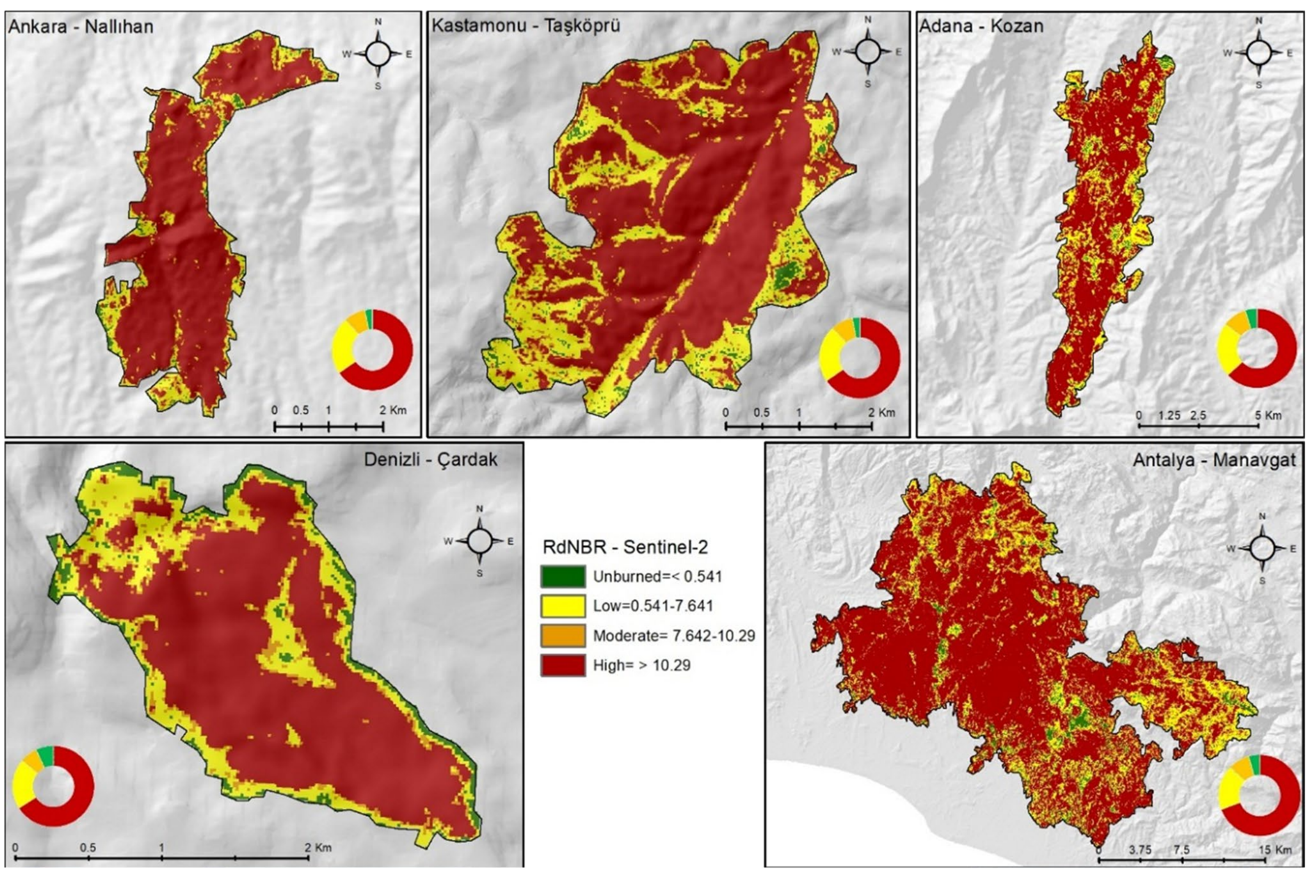

Fig. 7 Fire severity maps according to the Sentinel-2 based RdNBR thresholds

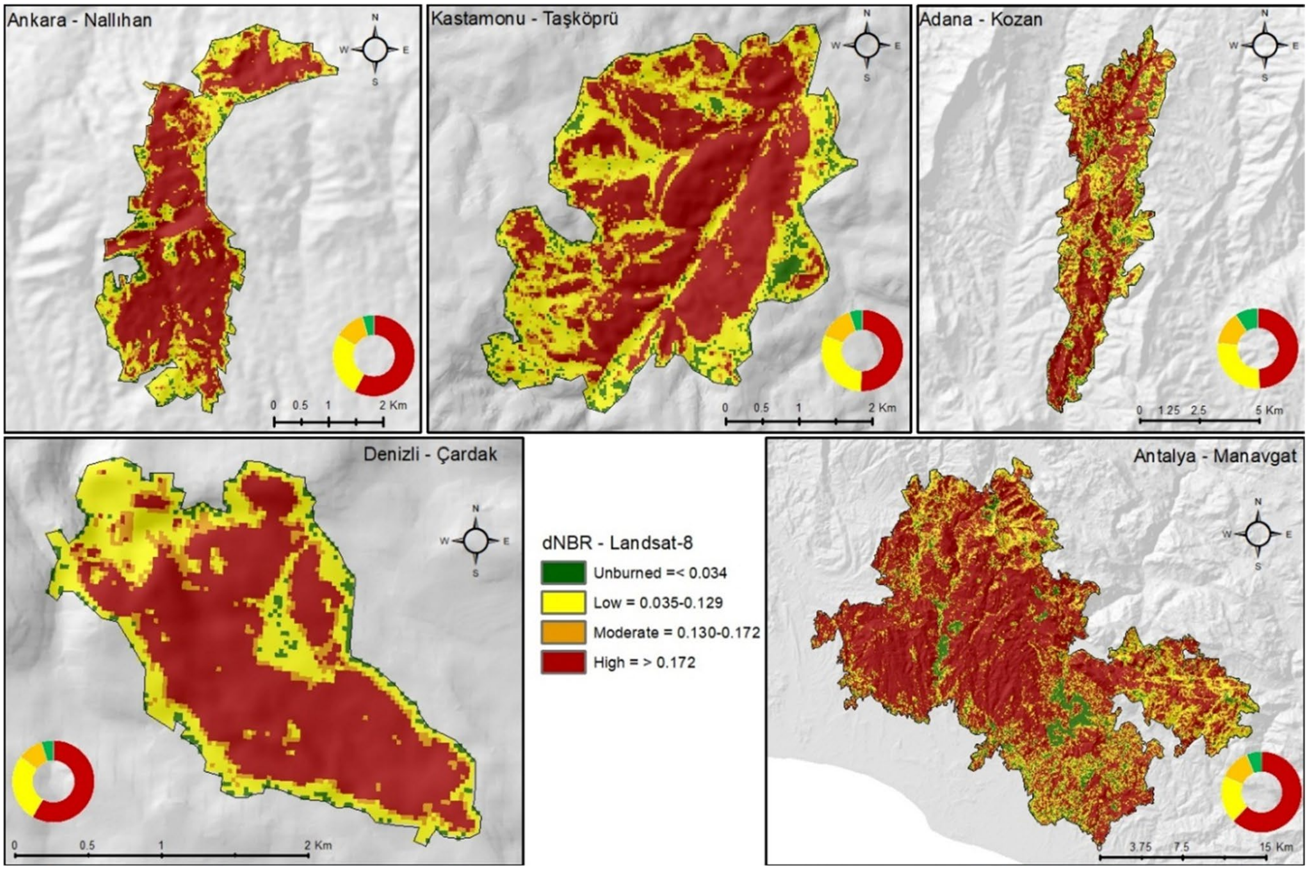

Fig. 8 Fire severity maps according to the Landsat-8 based dNBR thresholds

Conclusions

Fire severity maps are used to describe fire effects on flora and fauna habitats, soil, water systems, atmosphere, and society. They assist forest managers in post-fire decision-making processes. This study evaluated the performance of field-based estimates (CBI and GeoCBI) and spectral indices derived from Sentinel-2, Landsat-8/OLI, and MODIS images to assess fire severity in heterogeneous forest ecosystems of Turkey. Classification thresholds were calculated for well-performing indices and used for fire severity mapping. According to the results, regardless of the satellite used, NBR-based RdNBR and dNBR indices estimated fire severity more accurately than indices based on RED and NIR bands. While Sentinel-2 and Landsat-8/OLI images produced similar good results, MODIS's performed poorly. GeoCBI was closely related to spectral reflectance values than CBI and thus provided more reliable field measurements of fire severity. Spectral reflectance values can vary substantially depending on fire intensity, vegetation cover and species-specific reaction to the fire, and thus can cause regional differences when determining fire severity. This is why threshold values for dNBR in this study differ from those of other studies. Our results can be used in forest ecosystems with vegetation similar to that in this study and might also guide further research. Further, in order to better understand the effects of fire, especially in patchy, heterogeneous forest ecosystems, further research is needed from different regions and fire types, testing and validating fire severity maps based on remote sensing data.

Data availability The data that support this study will be shared upon reasonable request to the corresponding author.

Declarations

Conflict of interest The authors declare that they have no conflict of interest.

References

Alleaume S, Hely C, Le Roux J, Korontzi S, Swap RJ, Shugart HH, Justice CO (2005) Using MODIS to evaluate heterogeneity of biomass burning in southern African savannahs: a case study in Etosha. Int J Remote Sens 26(19):4219–4237. https://doi.org/10.1080/01431160500113492

Allen JL, Sorbel B (2008) Assessing the differenced normalized burn ratio's ability to map burn severity in the boreal forest and tundra ecosystems of Alaska's national parks. Int J Wildland Fire 17(4):463–475. https://doi.org/10.1071/WF08034

Amatulli G, Camia A, San-Miguel-Ayanz J (2013) Estimating future burned areas under changing climate in the EU-Mediterranean countries. Sci Total Environ 450:209–222. https://doi.org/10.1016/j.scitotenv.2013.02.014

Ariza A, Rey JS, de Miguel SM (2019) Comparison of maximum likelihood estimators and regression models for burn severity mapping in Mediterranean forests using Landsat TM and ETM+ data. Rev Cartogr. https://doi.org/10.35424/rcarto.i98.145

Arnett JTTR, Coops NC, Daniels LD, Falls RW (2015) Detecting forest damage after a low-severity fire using remote sensing at multiple scales. Int J Appl Earth Obs Geoinf 35:239–246. https://doi.org/10.1016/j.jag.2014.09.013

Ba R, Song W, Lo S, Xie Z (2020) Spectral characteristic analysis of burned area based on MODIS Data. In: Wu GY, Tsai KC, Chow WK (eds) The proceedings of 11th Asia-Oceania symposium on fire science and technology. AOSFST 2018. Springer, Singapore, pp 391–404. https://doi.org/10.1007/978-981-32-9139-3_29

Baysal İ, Bilgili E, Başkent EZ (2016) Orman yanginlari ve orman amenajman planlari. Kast Üniv Orman Fak Derg 16(1):169–180. https://doi.org/10.17475/kujff.48428

Beltrán-Marcos D, Suárez-Seoane S, Fernández-Guisuraga JM, Fernández-García V, Pinto R, García-Llamas P, Calvo L (2021) Mapping soil burn severity at very high spatial resolution from unmanned aerial vehicles. Forests 12(2):179. https://doi.org/10.3390/f12020179

Borini Alves D, Montorio Llovería R, Pérez-Cabello F, Vlassova L (2018) Fusing Landsat and MODIS data to retrieve multispectral information from fire-affected areas over tropical savannah environments in the Brazilian Amazon. Int J Remote Sens 39(22):7919–7941. https://doi.org/10.1080/01431161.2018.1479790

Cansler CA, McKenzie D (2012) How robust are burn severity indices when applied in a new region? Evaluation of alternate field based and remote rensing methods. Remote Sens 4(2):456–483. https://doi.org/10.3390/rs4020456

Chen X, Vogelmann JE, Rollins M, Ohlen D, Key CH, Yang L, Huang C, Shi H (2011) Detecting post-fire burn severity and vegetation recovery using multitemporal remote sensing spectral indices and field-collected composite burn index data in a ponderosa pine forest. Int J Remote Sens 32(23):7905–7927. https://doi.org/10.1080/01431161.2010.524678

Choubin B, Solaimani K, Roshan MH, Malekian A (2017) Watershed classification by remote sensing indices: a fuzzy c-means clustering approach. J Mt Sci 14(10):2053–2063. https://doi.org/10.1007/s11629-017-4357-4

Chuvieco E, Martin MP, Palacios A (2002) Assessment of different spectral indices in the red-near-infrared spectral domain for burned land discrimination. Int J Remote Sens 23(23):5103–5110. https://doi.org/10.1080/01431160210153129

Chuvieco E, Mouillot F, van der Werf GR, San Miguel J, Tanasse M, Koutsias N, García M, Yebra M, Padilla M, Gitas I (2019) Historical background and current developments for mapping burned area from satellite Earth observation. Remote Sens Environ 225:45–64. https://doi.org/10.1016/j.rse.2019.02.013

Cochrane MA, Ryan KC (2009) Fire and fire ecology: Concepts and principles. In: Cochrane MA (ed) Tropical Fire Ecology. Springer, Chichester, pp 25–62. https://doi.org/10.1007/978-3-540-77381-8_2

De Santis A, Chuvieco E (2009) GeoCBI: a modified version of the composite burn index for the initial assessment of the short-term burn severity from remotely sensed data. Remote Sens Environ 113(3):554–562. https://doi.org/10.1016/j.rse.2008.10.011

Epting J, Verbyla D, Sorbel B (2005) Evaluation of remotely sensed indices for assessing burn severity in interior Alaska using Landsat TM and ETM+. Remote Sens Environ 96(3–4):328–339. https://doi.org/10.1016/j.rse.2005.03.002

Escuin S, Navarro R, Fernandez P (2008) Fire severity assessment by using NBR (normalized burn ratio) and NDVI (normalized difference vegetation index) derived from LANDSAT TM/ETM images. Int J Remote Sens 29(4):1053–1073. https://doi.org/10.1080/01431160701281072

Fernández-García V, Santamarta M, Fernández-Manso A, Quintano C, Marcos E, Calvo L (2018) Burn severity metrics in fire-prone pine ecosystems along a climatic gradient using Landsat imagery. Remote Sens Environ 206:205–217. https://doi.org/10.1016/j.rse.2017.12.029

Fernández-Manso A, Fernández-Manso O, Quintano C (2016) SENTİNEL-2A red-edge spectral indices suitability for discriminating burn severity. Int J Appl Earth Obs Geoinf 50:170–175. https://doi.org/10.1016/j.jag.2016.03.005

Fornacca D, Ren G, Xiao W (2018) Evaluating the best spectral indices for the detection of burn scars at several post-fire dates in a mountainous region of Northwest Yunnan, China. Remote Sens 10(8):1196. https://doi.org/10.3390/rs10081196

French NH, Kasischke ES, Hall RJ, Murphy KA, Verbyla DL, Hoy EE, Allen JL (2008) Using Landsat data to assess fire and burn severity in the North American boreal forest region: an overview and summary of results. Int J Wildland Fire 17(4):443–462. https://doi.org/10.1071/WF08007

Gao B-C (1996) NDWI—a normalized difference water index for remote sensing of vegetation liquid water from space. Remote Sens Environ 58(3):257–266. https://doi.org/10.1016/S0034-4257(96)00067-3

García-Llamas P, Suárez-Seoane S, Fernández-Guisuraga JM, Fernández-García V, Fernández-Manso A, Quintano C, Taboada A, Marcos E, Calvo L (2019) Evaluation and comparison of Landsat 8, Sentinel-2 and Deimos-1 remote sensing indices for assessing burn severity in Mediterranean fire-prone ecosystems. Int J Appl Earth Obs Geoinf 80:137–144. https://doi.org/10.1016/j.jag.2019.04.006

Gascon F, Ramoino F (2017, April). Sentinel-2 data exploitation with ESA's sentinel-2 toolbox. In: EGU general assembly conference abstracts, p 19548

Hoscilo A, Tansey KJ, Page SE (2013) Post-fire vegetation response as a proxy to quantify the magnitude of burn severity in tropical peatland. Int J Remote Sens 34(2):412–433. https://doi.org/10.1080/01431161.2012.709328

Hoy EE, French NHF, Turetsky MR, Trigg SN, Kasischke ES (2008) Evaluating the potential of Landsat TM/ETM+ imagery for assessing fire severity in Alaskan black spruce forests. Int J Wildland Fire 17(4):500–514. https://doi.org/10.1071/WF08107

Huang H, Roy D, Boschetti L, Zhang H, Yan L, Kumar S, Gomez-Dans J, Li J (2016) Separability analysis of Sentinel-2A

multi-spectral instrument (MSI) data for burned area discrimination. Remote Sens 8(10):873. https://doi.org/10.3390/rs8100873
Hudak AT, Morgan P, Bobbitt MJ, Smith AMS, Lewis SA, Lentile LB, Robichaud PR, Clark JT, McKinley RA (2007) The relationship of multispectral satellite imagery to immediate fire effects. Fire Ecol 3(1):64–90. https://doi.org/10.4996/fireecology.0301064
Huete AR (1988) A soil-adjusted vegetation index (SAVI). Remote Sens Environ 25(3):295–309. https://doi.org/10.1016/0034-4257(88)90106-X
Huete A, Didan K, Miura T, Rodriguez EP, Gao X, Ferreira LG (2002) Overview of the radiometric and biophysical performance of the MODIS vegetation indices. Remote Sens Environ 83(1–2):195–213. https://doi.org/10.1016/S0034-4257(02)00096-2
Ilori CO, Pahlevan N, Knudby A (2019) Analyzing performances of different atmospheric correction techniques for Landsat 8: application for coastal remote sensing. Remote Sens 11(4):469. https://doi.org/10.3390/rs11040469
Itten KI, Meyer P (1993) Geometric and radiometric correction of TM data of mountainous forested areas. IEEE Trans Geosci Remote Sens 31(4):764–770. https://doi.org/10.1109/36.239898
Kasischke ES, Bruhwiler LP (2002) Emissions of carbon dioxide, carbon monoxide, and methane from boreal forest fires in 1998. J Geophys Res Atmos. https://doi.org/10.1029/2001JD000461
Kaufman YJ, Sendra C (1988) Algorithm for automatic atmospheric corrections to visible and near-IR satellite imagery. Int J Remote Sens 9(8):1357–1381. https://doi.org/10.1080/01431168808954942
Keeley JE (2009) Fire intensity, fire severity and burn severity: a brief review and suggested usage. Int J Wildland Fire 18(1):116–126. https://doi.org/10.1071/WF07049
Key CH (2006) Ecological and sampling constraints on defining landscape fire severity. Fire Ecol 2(2):34–59. https://doi.org/10.4996/fireecology.0202034
Key CH, Benson NC (2006) Landscape assessment (LA). In: Lutes DC (ed) FIREMON: fire effects monitoring and inventory system. US Department of Agriculture, Forest Service, Rocky Mountain Research Station, Fort Collins, pp LA-1–55. https://doi.org/10.2737/RMRS-GTR-164
Korhonen L, Packalen P, Rautiainen M (2017) Comparison of Sentinel-2 and Landsat 8 in the estimation of boreal forest canopy cover and leaf area index. Remote Sens Environ 195:259–274. https://doi.org/10.1016/j.rse.2017.03.021
Lasaponara R, Lanorte A, Pignatti S (2006) Multiscale fuel type mapping in fragmented ecosystems: preliminary results from hyperspectral MIVIS and multispectral Landsat TM data. Int J Remote Sens 27(3):587–593. https://doi.org/10.1080/01431160500227631
Lewis SA, Lentile LB, Hudak AT, Robichaud PR, Morgan P, Bobbitt MJ (2007) Mapping ground cover using hyperspectral remote sensing after the 2003 Simi and Old wildfires in Southern California. Fire Ecol 3(1):109–128. https://doi.org/10.4996/fireecology.0301109
Liu Z, Yang J, Dwomoh F (2016) Mapping recent burned patches in Siberian larch forest using Landsat and MODIS data. Eur J Remote Sens 49(1):861–887. https://doi.org/10.5721/EuJRS20164945
Lunetta RS, Elvidge C (1999) Remote sensing change detection: environmental monitoring methods and applications. CRC Press, Florida, pp 318
Luo H, Wu J (2022) An assessment of the suitability of Sentinel-2 data for identifying burn severity in areas of low vegetation. J Indian Soc Remote Sens. https://doi.org/10.1007/s12524-022-01518-7
Lutes DC, Keane RE, Caratti J F, Key CH, Benson NC, Sutherland S, Gangi LJ (2006) FIREMON: fire effects monitoring and inventory system (Gen. Tech. Rep. RMRS-GTR-164). FS Department of Agriculture, Rocky Mountain Research Station, Fort Collins, USA. https://doi.org/10.2737/RMRS-GTR-164
Mallinis G, Mitsopoulos I, Chrysafi I (2018) Evaluating and comparing Sentinel 2A and Landsat-8 operational land imager (OLI) spectral indices for estimating fire severity in a Mediterranean pine ecosystem of Greece. Gisci Remote Sens 55(1):1–18. https://doi.org/10.1080/15481603.2017.1354803
Matthew MW, Adler-Golden SM, Berk A, Felde G, Anderson GP, Gorodetzky D, Paswaters S, Shippert M (2002) Atmospheric correction of spectral imagery: evaluation of the FLAASH algorithm with AVIRIS data. In: Applied imagery pattern recognition workshop, pp 157–163
McCarley TR, Smith AMS, Kolden CA, Kreitler J (2018) Evaluating the Mid-Infrared Bi-spectral Index for improved assessment of low-severity fire effects in a conifer forest. Int J Wildland Fire 27(6):407. https://doi.org/10.1071/wf17137
Michaletz ST, Johnson EA (2007) How forest fires kill trees: a review of the fundamental biophysical processes. Scand J for Res 22(6):500–515. https://doi.org/10.1080/02827580701803544
Miller JD, Quayle B (2015) Calibration and validation of immediate post-fire satellite-derived data to three severity metrics. Fire Ecol 11(2):12–30. https://doi.org/10.4996/fireecology.1102012
Miller JD, Thode AE (2007) Quantifying burn severity in a heterogeneous landscape with a relative version of the delta normalized burn ratio (dNBR). Remote Sens Environ 109(1):66–80. https://doi.org/10.1016/j.rse.2006.12.006
Miller JD, Knapp EE, Key CH, Skinner CN, Isbell CJ, Creasy RM, Sherlock JW (2009) Calibration and validation of the relative differenced normalized burn ratio (RdNBR) to three measures of fire severity in the Sierra Nevada and Klamath Mountains, California, USA. Remote Sens Environ 113(3):645–656. https://doi.org/10.1016/j.rse.2008.11.009
Papageorgiou K, Hadjimitsis DG, Agapiou A, Themistocleous K, Koutsias N, Chrysoulakis N (2012) Spectral signatures of *Pinus brutia* post fire regeneration in Paphos forest, using ground spectroradiometers. In: Conference: 32nd EARSeL symposium, pp 223–230
Parker BM, Lewis T, Srivastava SK (2015) Estimation and evaluation of multi-decadal fire severity patterns using Landsat sensors. Remote Sens Environ 170:340–349. https://doi.org/10.1016/j.rse.2015.09.014
Parks SA, Dillon GK, Miller C (2014) A new metric for quantifying burn severity: the relativized burn ratio. Remote Sens 6(3):1827–1844. https://doi.org/10.3390/rs6031827
Pinty B, Verstraete M (1992) GEMI: a non-linear index to monitor global vegetation from satellites. Vegetatio 101(1):15–20. https://doi.org/10.1007/BF00031911
Pleniou M, Koutsias N (2013) Sensitivity of spectral reflectance values to different burn and vegetation ratios: a multi-scale approach applied in a fire affected area. ISPRS J Photogramm Remote Sens 79:199–210. https://doi.org/10.1016/j.isprsjprs.2013.02.016
Pletsch MAJS, Penha TV, Junior CHLS, Morelli F (2019) Combination of spectral indices for burned area detection in the Brazilian Amazonia. In: XIX Brazilian symposium on remote sensing, pp 1248–1251
Rogan J, Franklin J (2001) Mapping wildfire burn severity in southern California forests and shrublands using enhanced thematic mapper imagery. Geocarto Int 16(4):91–106. https://doi.org/10.1080/10106040108542218
Saulino L, Rita A, Migliozzi A, Maffei C, Allevato E, Garonna AP, Saracino A (2020) Detecting burn severity across Mediterranean forest types by coupling medium-spatial resolution satellite imagery and field data. Remote Sens 12(4):741. https://doi.org/10.3390/rs12040741
Smith A, Drake N, Wooster M, Hudak A, Holden Z, Gibbons C (2007) Production of Landsat ETM+ reference imagery of burned areas

within Southern African savannahs: comparison of methods and application to MODIS. Int J Remote Sens 28(12):2753–2775. https://doi.org/10.1080/01431160600954704

Song X-P, Huang W, Hansen MC, Potapov P (2021) An evaluation of Landsat, Sentinel-2, Sentinel-1 and MODIS data for crop type mapping. Sci Remote Sens. https://doi.org/10.1016/j.srs.2021.100018

Soverel NO, Perrakis DDB, Coops NC (2010) Estimating burn severity from Landsat dNBR and RdNBR indices across western Canada. Remote Sens Environ 114(9):1896–1909. https://doi.org/10.1016/j.rse.2010.03.013

Teillet PM (1986) Image correction for radiometric effects in remote sensing. Int J Remote Sens 7(12):1637–1651. https://doi.org/10.1080/01431168608948958

Trigg S, Flasse S (2001) An evaluation of different bi-spectral spaces for discriminating burned shrub-savannah. Int J Remote Sens 22(13):2641–2647. https://doi.org/10.1080/01431160110053185

Tucker CJ (1979) Red and photographic infrared linear combinations for monitoring vegetation. Remote Sens Environ 8(2):127–150. https://doi.org/10.1016/0034-4257(79)90013-0

Turner MG, Romme WH (1994) Landscape dynamics in crown fire ecosystems. Landsc Ecol 9(1):59–77. https://doi.org/10.1007/BF00135079

Valor T, González-Olabarria JR, Piqué M, Casals P (2017) The effects of burning season and severity on the mortality over time of *Pinus nigra* spp. *salzmannii* (Dunal) Franco and *P. sylvestris* L. For Ecol Manag 406:172–183. https://doi.org/10.1016/j.foreco.2017.08.027

Veraverbeke S, Lhermitte S, Verstraeten WW, Goossens R (2011) Evaluation of pre/post-fire differenced spectral indices for assessing burn severity in a Mediterranean environment with Landsat Thematic Mapper. Int J Remote Sens 32(12):3521–3537. https://doi.org/10.1080/01431161003752430

White JD, Ryan KC, Key CC, Running SW (1996) Remote sensing of forest fire severity and vegetation recovery. Int J Wildland Fire 6(3):125–136. https://doi.org/10.1071/WF9960125

Whitman E, Batllori E, Parisien MA, Miller C, Coop JD, Krawchuk MA, Chong GW, Haire SL (2015) The climate space of fire regimes in north-western North America. J Biogeogr 42(9):1736–1749. https://doi.org/10.1111/jbi.12533

Wilson EH, Sader SA (2002) Detection of forest harvest type using multiple dates of Landsat TM imagery. Remote Sens Environ 80(3):385–396. https://doi.org/10.1016/S0034-4257(01)00318-2

Wu Z, Middleton B, Hetzler R, Vogel J, Dye D (2015) Vegetation burn severity mapping using Landsat-8 and WorldView-2. Photogramm Eng Remote Sens 81(2):143–154. https://doi.org/10.14358/PERS.81.2.143

Ye H, Chen C, Yang C (2016) Atmospheric correction of Landsat-8/OLI imagery in turbid estuarine waters: a case study for the Pearl River estuary. IEEE J Sel Top Appl Earth Observations Remote Sens 10(1):252–261. https://doi.org/10.1109/JSTARS.2016.2614814

Zhu Z, Key C, Ohlen D, Benson N (2006) Evaluate sensitivities of burn severity mapping algorithms for different ecosystems and fire histories in the United States. Final Report to the Joint Fire Science Program (JFSP Project No. 01-1-4-12). USGS, Sioux Falls, USA. https://www.frames.gov/catalog/391